Hydrophobic gasket mutation produces gating pore currents in closed human voltage-gated proton channels

Richard Banh[a,b], Vladimir V. Cherny[c], Deri Morgan[c], Boris Musset[d], Sarah Thomas[e], Kethika Kulleperuma[a], Susan M. E. Smith[e], Régis Pomès[a,b,1], and Thomas E. DeCoursey[c,1]

[a]Molecular Medicine, Hospital for Sick Children, Toronto, ON M5G 1X8, Canada; [b]Department of Biochemistry, University of Toronto, Toronto, ON M5S 1A8, Canada; [c]Department of Physiology and Biophysics, Rush University, Chicago, IL 60612; [d]Institut für Physiologie und Pathophysiologie, Paracelsus Medizinische Privatuniversität, 90419 Nürnberg, Germany; and [e]Department of Molecular and Cellular Biology, Kennesaw State University, Kennesaw, GA 30144

Edited by Michael D. Cahalan, University of California, Irvine, CA, and approved August 1, 2019 (received for review March 29, 2019)

The hydrophobic gasket (HG), a ring of hydrophobic amino acids in the voltage-sensing domain of most voltage-gated ion channels, forms a constriction between internal and external aqueous vestibules. Cationic Arg or Lys side chains lining the S4 helix move through this "gating pore" when the channel opens. S4 movement may occur during gating of the human voltage-gated proton channel, hH_V1, but proton current flows through the same pore in open channels. Here, we replaced putative HG residues with less hydrophobic residues or acidic Asp. Substitution of individuals, pairs, or all 3 HG positions did not impair proton selectivity. Evidently, the HG does not act as a secondary selectivity filter. However, 2 unexpected functions of the HG in H_V1 were discovered. Mutating HG residues independently accelerated channel opening and compromised the closed state. Mutants exhibited open–closed gating, but strikingly, at negative voltages where "normal" gating produces a nonconducting closed state, the channel leaked protons. Closed-channel proton current was smaller than open-channel current and was inhibited by 10 μM Zn^{2+}. Extreme hyperpolarization produced a deeper closed state through a weakly voltage-dependent transition. We functionally identify the HG as Val^{109}, Phe^{150}, Val^{177}, and Val^{178}, which play a critical and exclusive role in preventing H^+ influx through closed channels. Molecular dynamics simulations revealed enhanced mobility of Arg^{208} in mutants exhibiting H^+ leak. Mutation of HG residues produces gating pore currents reminiscent of several channelopathies.

HVCN1 | voltage-sensing domain | voltage gating | ion channels | protons

Voltage-gated proton channels (H_V1) exist in phylogenetically disparate species where they perform even more disparate functions, from calcification in coccolithophores (1) and mediating action potentials in bioluminescent dinoflagellates (2, 3), to numerous functions in various human tissues (4) such as compensating for electron flux in phagocytes (5–10) and enabling sperm capacitation (11). Identification of the gene (12, 13) revealed that H_V1 has 4 transmembrane helices, S1 to S4, and is homologous to the voltage-sensing domains (VSDs) present in most voltage-gated ion channels, voltage-sensing phosphatases, and TMEM266 (14). Unlike VSDs of other channels that sense voltage and cause a separate pore to open or close, H_V1 itself conducts protons (15), producing a direct readout of its gating state and making it a unique system for studying gating mechanisms.

Cysteine scanning studies of the aqueous accessibility of residues on the S4 helix of K^+ channels revealed that VSDs contain 2 aqueous vestibules that are separated by a relatively short isthmus, termed the hydrophobic gasket (HG), within which S4 residues are inaccessible from either side of the membrane (16–18). In *Shaker* K^+ channels, replacing each of the first 4 Arg in S4 individually with His further revealed that in each case anomalous proton transfer, by carrier or channel mechanisms, occurred within a specific voltage range (19–21). These results suggested that a proton, presumably as a hydronium ion, can access the HG at the center of the "gating pore" where the imidazole group of His accepts the proton, perhaps rotates, and then protonates a water molecule on the distal side.

Several amino acids contributing to the HG in *Shaker* K^+ channels were identified, including I237 on S1 and F290 on S2 (22, 23); these positions correspond to Val^{109} and Phe^{150} in hH_V1. The same highly conserved Phe in S2 together with 2 conserved acidic groups (Asp^{174} and Glu^{153} in hH_V1) was proposed to act as a "charge transfer center" that temporarily stores each cationic group (Arg or Lys) in the *Shaker* S4 segment as it moves from the internal vestibule to the external vestibule (24). That hH_V1 shares the architectural feature of a short hydrophobic barrier is suggested by the R205H mutant in which the His shuttles protons into the cell at negative voltages (25), and by efficient proton permeation through open channels.

The *Ciona intestinalis* voltage-sensing phosphatase (CiVSP) is more closely related to H_V1 phylogenetically than are K^+ channels (3). Crystal structures of CiVSP were determined in both "down" and "up" positions, corresponding with closed and

Significance

A large family of membrane proteins, voltage-gated ion channels, regulate a vast array of physiological functions in essentially all life forms. How these molecules sense membrane potential and respond by creating ionic conduction is incompletely understood. The voltage sensors of these channels contain a "hydrophobic gasket," a ring of hydrophobic amino acids near the center of the membrane, separating internal and external aqueous solutions. Although voltage-gated proton channels, H_V1, resemble voltage-sensing domains of other channels, they differ fundamentally. On depolarization, H_V1 conducts protons, whereas other voltage sensors open a physically distinct pore. We identify Val^{109}, Phe^{150}, Val^{177}, and Val^{178} as the hH_V1 hydrophobic gasket. Replacement with less hydrophobic amino acids accelerated channel opening and caused proton-selective leak through closed channels.

Author contributions: S.M.E.S., R.P., and T.E.D. designed research; V.V.C., D.M., and B.M. performed research; R.B. and K.K. performed molecular dynamics calculations; R.P. supervised molecular dynamics calculations; S.T. and S.M.E.S. contributed new reagents/analytic tools; V.V.C., D.M., B.M., and S.T. analyzed data; and R.B., S.M.E.S., R.P., and T.E.D. wrote the paper.

The authors declare no conflict of interest.

This article is a PNAS Direct Submission.

[1]To whom correspondence may be addressed. Email: pomes@sickkids.ca or tdecours@rush.edu.

This article contains supporting information online at www.pnas.org/lookup/suppl/doi:10.1073/pnas.1905462116/-/DCSupplemental.

Published online August 28, 2019.

open states (26). Li et al. (27) also studied hH_V1 using electron paramagnetic resonance (EPR) and produced closed and open models of hH_V1 based on the CiVSP structures. These studies identified 3 conserved hydrophobic amino acids (Val^{109}, Phe^{150}, and Val^{178}) (28) as plausible members of the HG in hH_V1. The positions of S1 and S4, but not S2 and S3, in the hH_V1 models corresponded well with the single existing crystal structure of H_V1 in a presumed closed state. In the chimeric molecule successfully crystallized (29), the cytoplasmic ends of S2 and S3 segments of the mouse channel were replaced with the corresponding section of CiVSP. Li et al. (27) concluded that if S3 in the mH_V1 crystal were shifted upward (toward the extracellular surface) and S2 downward by 1 helical turn, the structure and model would match. A significant consequence is that, in the mH_V1 crystal structure, the third HG residue is predicted to be Phe^{182}, not Val^{178} (both with hH_V1 numbering). Fig. 1 illustrates the location of the putative HG residues in the homology model and crystal structure of hH_V1 in relation to other important amino acids, including Asp^{112} that is required for proton selectivity (30) and Arg^{208}, the central of 3 Arg in the S4 helix that contribute to gating charge (31).

Here, we address both the identity of amino acids contributing to, and the functional importance of, the HG in hH_V1 by replacing several amino acids in this region with neutral but smaller and less hydrophobic ones, or with Asp, which may be charged. The results reaffirm that hH_V1 contains a narrow barrier separating internal and external solutions like other VSDs, but in addition the HG ensures the occlusion of protons in the closed channel. We mutated both Val^{178} and Phe^{182} to determine which is more likely to be a member of the HG by exploiting our discovery of distinctive effects of mutating Val^{109} and Phe^{150}. This approach identified Val^{178} and another HG residue, Val^{177}.

Results

Experimental Strategy. Molecular dynamics (MD) simulations of a homology model of the open state of hH_V1 (33) were performed, and mutations designed to compromise the integrity of the HG were proposed for experimental testing. Increased pore hydration and a lowered barrier in the potential of mean force for the movement of Na^+ along the channel suggested that some of these mutants might be permeable to Na^+ in the open state (*SI Appendix*, Fig. S1 and Table S1). When these mutants were tested experimentally, the channel did not conduct Na^+ (Table 1) but was discovered to be leaky to H^+ in the closed state.

In order to evaluate the role and importance of the HG in hH_V1, we mutated the putative HG residues themselves (V109, F150, and V178) as well as several nearby hydrophobic amino acids (Fig. 1). Specifically, L108 and V177 neighbor putative HG positions; I105, L147, and F182 are 1 tier below or above the HG in our model. We mutated one or more HG residues to less hydrophobic and smaller amino acids, or to the negatively charged Asp. The background was the full-length wild-type (WT) hH_V1, which assembles as a dimer. Distinctive features common to the last 10 constructs in Table 1 are discussed using F150D and V109D as examples. The similar phenomenology of these mutants reinforces the idea that their behavior is a consequence of decreased hydrophobicity.

Lower Hydrophobicity at the HG Did Not Impair H^+ Selectivity. For each construct, voltage-clamp current families were collected at several pH to evaluate the general effects of the mutation. Essentially all hH_V1 mutants studied were strongly proton selective (Table 1). Selectivity was assessed by determining the reversal potential, V_{rev}, at several pH. For most mutants in the upper half of the table, changes in pH_o (in whole-cell studies) or pH_i (in inside-out patch studies) shifted V_{rev} by ≥50 mV/unit, which indicates H^+ selectivity. Imperfect pH control accounts for deviations from the Nernst potential for H^+ (34, 35). We specifically examined possible Na^+ permeability. Changing the predominant cation from TMA^+ to Na^+ shifted V_{rev} by only a few millivolts, within the range of liquid junction potentials, which we consider negligible. Replacing TMA^+ with Na^+ should shift V_{rev} by

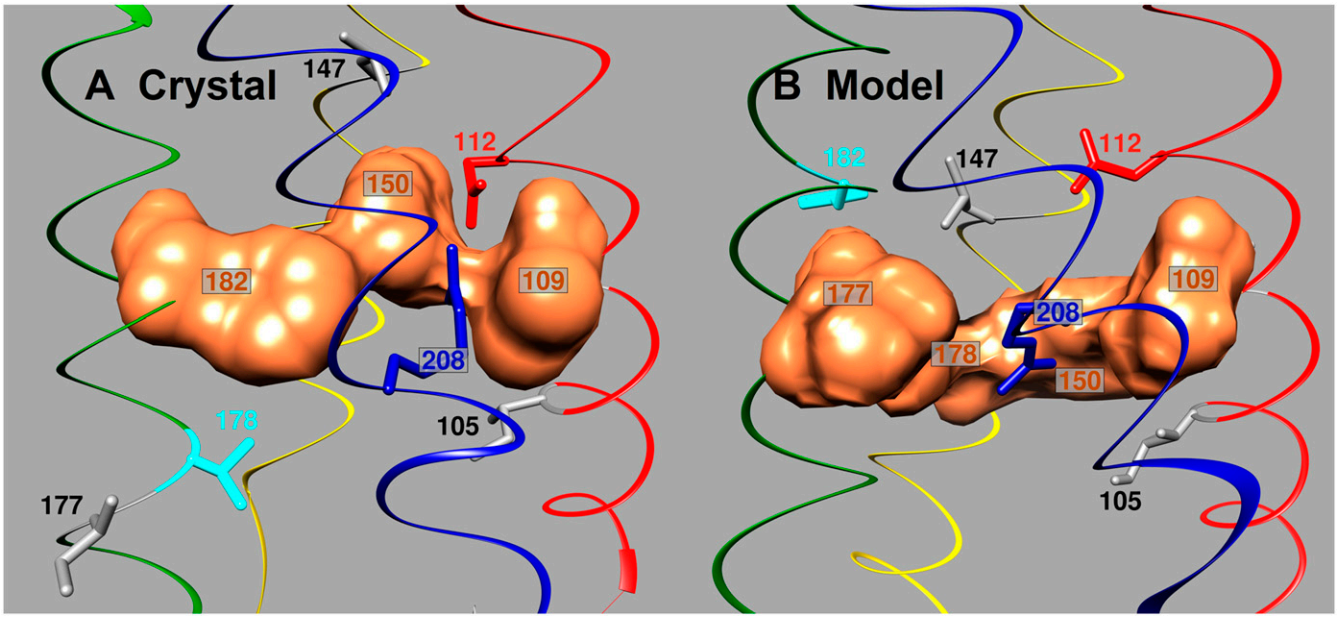

Fig. 1. Close-up side view of the central region of H_V1 in a closed state (*A*) in the crystal structure, and (*B*) in the model of Li et al. (27). Structures were superimposed and are shown at the same viewing angle. The putative HG residues (surface representation of side chains in bronze) are V109, F150, and F182 in the crystal structure (human numbering), but V109, F150, V177, and V178 in the model; the disputed element in each is aqua. Asp^{112} is red, Arg^{208} in S4 is blue, and other residues mutated here are gray. Helices are color-coded: S1, red; S2, yellow; S3, green; S4, blue. Extracellular is above. Superimposed and drawn with the University of California, San Francisco (UCSF) Chimera package (Resource for Biocomputing, Visualization, and Informatics, UCSF, supported by National Institute of General Medical Sciences Grant P41-GM103311) (32).

Table 1. Closed channel conductance and selectivity of HG mutants

Mutant	$g_{H,closed}$	g_H(C/O) pH 7	ΔV_{rev} pH 7→6	ΔV_{rev} pH 7→8	ΔV_{rev} pH 6→5	ΔV_{rev} TMA^+→Na^+
I105G	No	0	56.7 ± 1.6 (6)	53.7 ± 3.5 (5)		—
I105D	No	0	49.4 ± 2.3 (5)	49 (1)	60 (1)	1.8 ± 0.8 (3)
L108T	No	0	53 (1)	55.5 ± 3.5 (2)		−2.4 (1)
V109T	No	0	52.8 ± 1.1 (4)	55.7 ± 1.9 (3)		1.6 (1)
V109A	No	0	56.5 ± 1.0 (4)		54.0 ± 6.0 (2)	1.1 ± 1.3 (3)
L147T	No	0	51.3 ± 3.0 (3)			—
L147D	No	0	50.7 ± 1.7 (3)	53 (1)		0.2 ± 0.4 (5)
F150A	No	0	47.5 ± 1.5 (2)	52 (1)		−0.5 ± 0.8 (4)
V178T	No	0	49 (1)			
F182A	No	0	55.8 ± 1.1 (4)	50.1 ± 3.0 (2)	45	−0.9 ± 1.1 (3)
V177T	No	0	47.0 ± 4.0 (3)	53.8 ± 2.5 (5)		−0.3 ± 1.0 (3)
V177D	Yes	0.103 ± 0.014 (8)	55.3 ± 3.7 (3)			0.5 ± 0.2 (3)
V178A	Yes	0.017 ± 0.010 (5)	50.2 ± 1.4 (4)	47 (1)		0.6 ± 0.7 (3)
V109A/F150A	Yes	0.164 ± 0.044 (6)	49.7 ± 3.8 (3)	34 (1)		0.8 ± 1.1 (4)
V109A/V178A	Yes	0.028 ± 0.012 (7)	49.9 ± 1.3 (4)			0.8 ± 0.8 (3)
F150A/V178A	Yes	0.144 ± 0.015 (3)	44.5 ± 0.5 (2)	70 (1)		−0.6 ± 0.6 (3)
V178D	Yes	0.036 ± 0.019 (4)	57.3 ± 1.4 (4)	50.7 ± 2.7 (3)	55 (1)	0.6 ± 1.2 (6)
V109A/F150A/V178A	Yes	0.35 ± 0.05 (9)	44.0 ± 2.8 (5)	36.3 ± 4.9 (3)	29.7 ± 11.9 (3)	−0.3 ± 0.4 (4)
V109D	Yes	0.40 ± 0.06 (5)	59 (1)			3.0 ± 0.9 (3)
F150D	Yes	0.38 ± 0.09 (4)	39.3 ± 3.5 (3)	45 (1)	39 ± 6 (2)	1.2 ± 1.4 (4)
F150D/R211G	Yes	0.67 ± 0.04 (6)	39.6 ± 8.2 (5)	33.3 ± 8.4 (4)	41.0 ± 6.4 (4)	1.8 ± 0.4 (5)

The existence of $g_{H,closed}$ was defined as consistent reversible changes in the holding current of >1 pA when pH was changed or with addition of Zn^{2+} or both. Absolute values of V_{rev} changes with pH are given for both whole-cell and inside-out patch measurements. Mutants with large $g_{H,closed}$ tend to have smaller and more variable V_{rev} changes with pH because proton leak at V_{hold} continually dissipates the pH gradient even if the channel is perfectly proton selective, to an extent dependent on geometry and other factors. Parameter g_H(C/O) is the ratio of closed to open g_H (*Materials and Methods*). Monovalent cation substitutions were done at pH 7//7, and measured liquid junction potentials have been corrected.

17.5 mV if P_H/P_{Na} were 10^6 and by 2.4 mV if P_H/P_{Na} were 10^7, calculated with the Goldman–Hodgkin–Katz voltage equation. We cannot rule out Na^+ permeation altogether; we simply cannot measure it.

Increasing the Hydrophilicity of the HG Compromises the Impermeability of the Closed Channel. Increasing the hydrophilicity of the HG impaired the ability of hH_V1 channel closure to occlude proton leak through the channel. Fig. 2 illustrates this dramatic consequence in the F150D mutant. Three families of currents in the same cell are shown, nominally at pH_o 7, pH_i 7. The family in Fig. 2*A* generally resembles WT hH_V1 currents, but with some differences. Time-dependent turn-on of outward current appears at 0 mV and above (~20 mV earlier than WT). Most remarkably, the cell appears leaky, with a substantial time-independent current at V_{hold} and with large instantaneous jumps at the start of each depolarizing pulse. Four kinds of evidence support the idea that this "leak" conductance ($g_{H,closed}$) is carried largely or entirely by protons through a closed state of the mutant proton channel. First, it was inhibited by Zn^{2+}. Zn^{2+} has no effect on leak current in cells transfected with WT hH_V1 (36). Fig. 2 *B* and *C* illustrates the inhibition of both open and closed F150D channels by 1 μM Zn^{2+} and 10 μM Zn^{2+}. The currents during pulses to +80 mV superimposed in Fig. 2*D* illustrate that the holding current at −40 mV, and the outward currents appear similarly sensitive to inhibition by Zn^{2+}. We interpret the inward current at −40 mV as closed-channel current, because time-dependent activation of proton current was evident only at 0 mV or more positive (Fig. 2*A*). We interpret the instantaneous jump in outward current during depolarizing pulses as current flowing through conducting closed channels, which is followed by a slow rise in current that we attribute to channels opening in a relatively normal time-dependent manner.

Second, the inward current at the holding potential V_{hold} lowered pH_i, consistent with proton-selective leak current. When inward current at V_{hold} was increased by removing Zn^{2+} (Fig. 2*E*) or lowering pH_o (Fig. 3), the test pulse current amplitude increased over several minutes as the greater proton influx lowered pH_i. This phenomenon made quantitative study of the properties of mutants displaying $g_{H,closed}$ quite difficult, because essentially all H_V1 properties depend strongly on pH. In general, constitutive g_H will act to dissipate the applied pH gradient. Because we typically held the membrane at negative voltages (to close the channels), the presence of a closed-channel g_H will tend to drive the Nernst potential for H^+, E_H, toward V_{hold}. At symmetrical pH_o 7, pH_i 7, E_H is nominally 0 mV, but continuous H^+ influx at V_{hold} will lower pH_i. Indeed, in 4 cells expressing F150D, the holding current at −40 mV averaged −49 ± 10 pA (mean ± SEM) and V_{rev} was −10.8 ± 1.6 mV. Measured by tail currents, V_{rev} became more negative when V_{hold} was more negative, because there was a larger steady H^+ influx. Fig. 2*E* illustrates the mutable nature of pH_i in these experiments. The record begins at symmetrical pH 7 (nominal) in the presence of 10 μM Zn^{2+}, which had greatly reduced both inward and outward currents. Application of pH_o 7 solution with EGTA to this cell relieved inhibition, rapidly increasing the inward holding current at −40 mV as well as the outward current during the +40-mV test pulses. The inward current then gradually decreased, reflecting a decreasing driving force as H^+ influx progressively lowered pH_i, moving E_H closer to V_{hold}. The progressive increase in outward current during the test pulses to +40 mV also results from the lower pH_i, which increases both g_H and the driving force (40 mV − V_{rev}). Changing the bath to pH_o 8 not only decreased the inward current at −40 mV but produced an overshoot of outward current, demonstrating that E_H was now well negative to −40 mV. The overshoot dissipated as H^+ efflux increased pH_i. This example shows clearly that H^+ flux through closed channels changes pH_i profoundly and that all numerical results presented here must be taken as approximate.

A third type of evidence of H^+-selective closed-channel conduction is that the magnitude of the leak at V_{hold} varied according to pH_o, as expected for changes in the permeant ion concentration. The current at V_{hold} increased at lower pH_o and

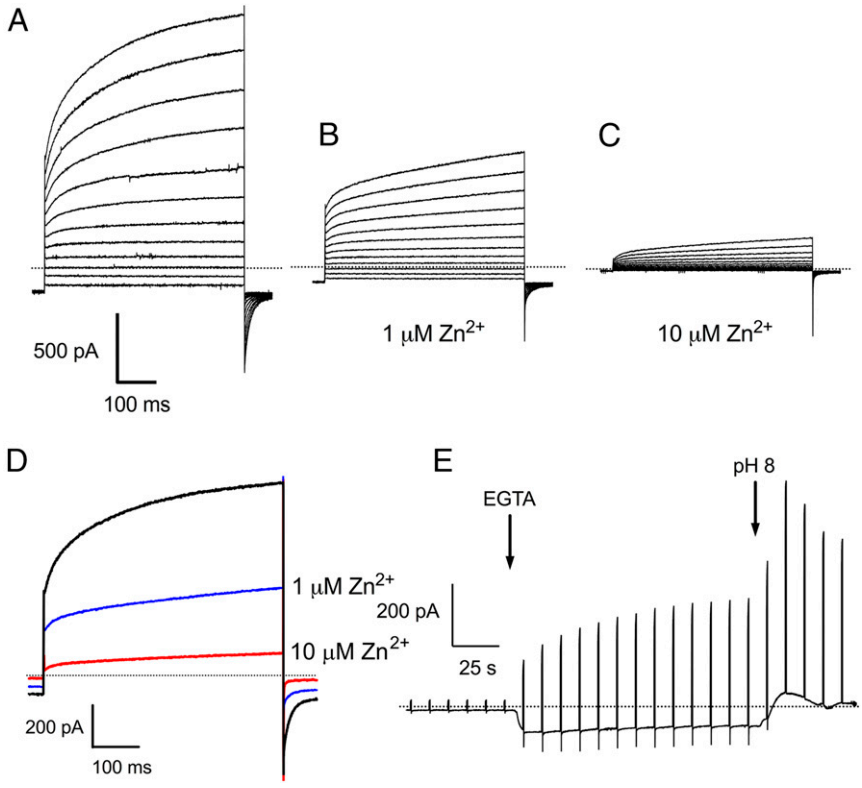

Fig. 2. Zn^{2+}-sensitive closed-channel proton conductance in a cell expressing the F150D mutant. (*A*) A family of currents elicited by pulses applied from V_{hold} = −40 mV to −30 through +80 mV in increments of 10 mV. The dotted line indicates zero current. The nominal pH was 7.0//7.0, but V_{rev} was −10 mV, indicating that pH_i was in fact 6.83. Families of currents at the same voltages in the same cell in the presence of 1 μM Zn^{2+} (*B*) or 10 μM Zn^{2+} (*C*) show substantial reduction of both inward and outward currents. (*D*) Superimposed currents at 80 mV in this cell reveal similar Zn^{2+} sensitivity of open and closed channels. Application of 1 μM Zn^{2+} or 10 μM Zn^{2+}, respectively, reduced the inward current at −40 mV to 57% and 8%, the initial current at the start of the pulse to 80 mV to 56% and 8%, and the current at the end of the pulse to 38% and 15%. (*E*) The time course of changes in closed-channel current at −40 mV and open-channel current during test pulses to 40 mV applied every 10 s in the same cell as *A*–*D*. Initially, the bath contained 10 μM Zn^{2+}. At the arrow, the bath was washed with pH 7 solution containing EGTA, producing both rapid and gradual changes. Then pH 8 solution was applied, resulting in outward current at −40 mV.

decreased at higher pH_o in whole-cell studies, consistent with protons being a major charge carrier. Figs. 2*E* and 3 illustrate this phenomenon in F150D and V109D mutants, respectively. The manifestations in inside-out patches were inverted, and the inward current at V_{hold} became smaller when pH_i was lowered. In cells lacking hH_V1 or with WT hH_V1, the leak current at V_{hold} did not change with pH_o. When pH_o was decreased in cells with V109D, closed-channel proton currents increased. Lowering pH_o from 5.5 to 4.5 (with nominally pH_i 5.5) increased the holding current at −40 or −60 mV by a factor 3.0 ± 0.2 in 5 cells (mean ± SEM), as illustrated in Fig. 3. However, correcting for the change in driving force decreases this difference. Evidently $g_{H,closed}$ increases as pH_o is lowered considerably less than in proportion to the proton concentration.

Finally, if HG mutant channels conduct protons selectively in both open and closed states, and any other conductances present are negligibly small, then the membrane should act as a pH electrode. This prediction is borne out in Fig. 4, which shows the effects of pH changes on membrane potential in a cell with V109D channels studied under current-clamp conditions. Beginning with symmetrical pH 5.5 solutions, the membrane potential was near 0 mV. Changing pH_o to 4.5 resulted in a rapid 40-mV depolarization that was reversed upon return to pH 5.5. Increasing pH_o to 6.5 hyperpolarized the membrane by a nearly Nernstian amount (∼58 mV/unit pH), showing that the membrane conductance is overwhelmingly proton selective. Returning to pH_o 5.5 resulted in rapid depolarization to ∼0 mV. Replacing $CH_3SO_3^-$ with Cl^- produced only a transient blip, indicating negligible anion permeability. Replacing TMA^+ with Na^+ or K^+ had similarly minor effects. That the membrane potential of this cell approached the Nernst potential for protons (E_H) and was minimally affected by other ions indicates that the conductance was proton selective. If a small fraction of channels remain open at V_{rev} (0 mV at symmetrical pH), the membrane potential changes most likely reflect proton conductance through a mixture of open and closed channels.

We tested the proton selectivity of closed channels by comparing the holding current in TMA^+ or Na^+ solutions at pH 7. Na^+ sometimes produced small increases in the holding current in some mutants, but these were insensitive to Zn^{2+}, which blocked $g_{H,closed}$ (Fig. 2). Furthermore, we sometimes saw similar effects of Na^+ in nontransfected HEK-293 cells. We conclude that closed hH_V1 channels are not detectably permeable to Na^+.

Estimating the Conductance of Closed Channels. Given that the existence of $g_{H,closed}$ changes pH_i and consequently V_{rev}, accurate conductance estimates are improbable. However, in cells in which 10 to 100 μM Zn^{2+} was applied (e.g., Fig. 2), typically up to 90% of the holding current was eliminated. The error is thus not inordinate. Rough estimates were obtained at symmetrical pH 7.0 in 2 ways (*Materials and Methods*). The holding current, usually at −40 or −60 mV, was considered to reflect mainly $g_{H,closed}$. The time-independent (or weakly time-dependent) currents at negative voltages reversed at very nearly the same

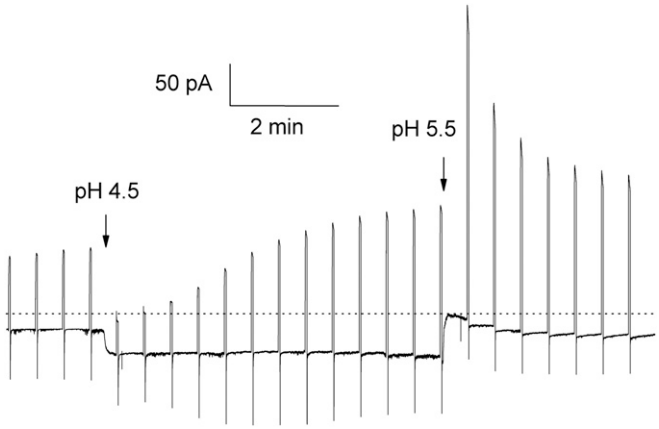

Fig. 3. Proton influx through closed V109D channels lowers pH_i. Whole-cell currents were recorded initially in symmetrical pH 5.5 solutions, with the membrane held at −60 mV and 2-s test pulses to 20 mV applied every 30 s. The arrows indicate when pH_o was changed. When pH_o was lowered from 5.5 to 4.5, the holding current increased immediately, reflecting proton influx through closed (C_1) channels. The test pulse current at 20 mV decreased at first, reflecting the positive shift of E_H (which decreases or even inverts the driving force) as well as the expected positive shift of the g_H–V relationship due to the ΔpH dependence of gating (37). However, during subsequent pulses the test current increased progressively as the H^+ influx that occurs continuously at V_{hold} lowered pH_i and reversed these 2 changes, resulting in both E_H and the g_H–V relationship shifting negatively over the course of several minutes. Eventually, the test current at 20 mV is even larger at pH_o 4.5 than it was at nominally symmetrical pH, presumably indicating that the true pH_i has dropped lower than it was initially at pH_o 5.5. Lowering pH_i increases g_H of WT H_V1 channels by roughly 2-fold/unit in most whole-cell studies of voltage-gated proton channels (38). Upon return to pH_o 5.5, the test current during the first pulse is much larger than it was previously in the same solution, reflecting the lower pH_i. The holding current at −60 mV rapidly approaches 0 pA, showing that the true pH gradient shortly after the bath change was roughly pH_o 5.5, pH_i 4.5, and thus E_H was near V_{hold} at −60 mV. Gradually, H^+ directly extruded by the large outward test pulse currents and decreased H^+ influx at V_{hold} restores pH_i toward its previous value.

voltage as the time-dependent "normal" g_H based on traditional tail current measurements, consistent with both being largely or entirely proton selective. In mutants with large $g_{H,closed}$, there was an instantaneous jump upon depolarization, which we ascribe to closed-channel conductance, followed by a slower time-dependent increase in current, which we attribute to the normal opening process. We assume that the time course reflects the increasing proportion of open channels, and the final current reflects the fully open-channel conductance.

The amplitude of $g_{H,closed}$ relative to the g_H of open channels is given in Table 1 as g_H(C/O). Replacing individual HG residues with Ala produced detectable $g_{H,closed}$ only for V178A. However, all 3 double Ala mutants (V109A/F150A, V109A/V178A, and F150A/V178A) leaked protons when closed, and the triple Ala mutant had a large leak with $g_{H,closed}$ one-third of the open conductance. Each HG residue replaced by Asp produced distinct $g_{H,closed}$.

A Deeper Closed State Revealed in V109D. Fig. 5*A* shows a typical family of V109D currents at symmetrical pH 5.5//5.5. From V_{hold} = −60 mV pulses to more negative voltages elicited slowly decaying inward currents. A superficial interpretation might be that these are "tail currents" due to a population of channels open at −60 mV that close at more negative voltages. Consistent with this idea, repolarization to −60 mV results in slowly activating inward currents, which are more obvious in Fig. 5*B*. Above about –30 mV, a proton conductance with more normal appearance begins to turn on. Its activation is faster than WT hH_V1, and the g_H appears to activate at somewhat more negative voltages. For reasons discussed above, we suspect that the apparently closed channels still conducted proton current, even at −60 mV. One consequence is that V_{rev} determined by tail currents in this cell was −28 mV. The continuous proton influx at V_{hold} lowered pH_i well below the nominal pH 5.5 of the pipette solution to ∼5.02.

Lowering pH_o shifts the g_H–V relationship of all known proton channels by ∼40 mV to more positive voltages (4, 37, 38). We therefore lowered pH_o to 4.5 (Fig. 5*B*), to ensure that all of the channels at V_{hold} were closed. The well-spaced currents at positive voltages now appear to activate about 40 mV more positively, with increased spacing above +10 mV, but the inward (proton-selective) holding current at −40 mV was increased, and the decaying inward currents during pulses to more negative voltages were more pronounced. Both from time-dependent relaxation of tail currents and the reversal of total current, V_{rev} was +21 mV, indicating that pH_i was now 4.86. Thus, V_{rev} shifted 49 mV when pH_o was lowered from 5.5 to 4.5, and ΔpH shifted by 0.84 units. The V_{rev} shift was thus 58.3 mV/unit (49 mV/0.84 units) indicating perfect proton selectivity. Examination of the tail currents seen upon repolarization at both pH_o reveal that, following pulses in the negative voltage range, the currents exhibit a monoexponential time course. Following depolarizing pulses that activate normal time-dependent outward currents, the tail currents are distinctly double exponential. The amplitudes of each kinetic component as well as their sum are plotted in Fig. 5*C*. The fast tail currents are associated with activation of the normal g_H and are steeply voltage dependent. The slow tail currents evidently reflect a slow gating process between closed but conducting channels and a deeper closed state that appears not to conduct detectably.

The behavior of V109D in Fig. 5 suggests the following gating transitions:

$$Closed_2 \underset{slow}{\overset{slow}{\rightleftharpoons}} Closed_1 \underset{fast}{\overset{slow}{\rightleftharpoons}} Open. \qquad [1]$$

The $Closed_2$ (C_2) state does not conduct or conducts negligibly. $Closed_1$ (C_1) and *Open* (O) both conduct protons but O has a higher conductance. The transition between C_2 and C_1 has very weak voltage dependence. The $C_1 \rightarrow O$ transition has strong voltage dependence that presumably reflects movement of most of the gating charge.

The experiment in *SI Appendix*, Fig. S2 provides additional evidence that $C_2 \leftrightarrow C_1$ transitions are kinetically distinct from the normal opening transition. Activation kinetics and amplitude depend on prepulse voltage. Similar behavior was observed in many cells expressing V109D, both at pH 7 and at pH 5.5. According to **[1]**, the most negative prepulses produce $C_2 \rightarrow C_1 \rightarrow O$ transitions,

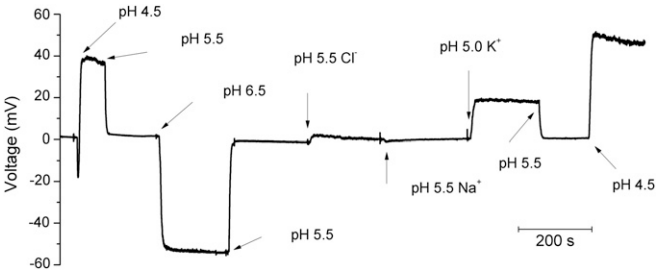

Fig. 4. Membrane potential response to pH changes in a cell with the V109D mutant confirms proton selectivity. The initial condition was symmetrical pH 5.5 TMA^+ $CH_3SO_3^-$ solutions, with membrane potential recorded under current clamp. At the arrows, pH_o was changed, Cl^- was substituted for $CH_3SO_3^-$, or Na^+ or K^+ (at pH 5.0) replaced TMA^+, as indicated. The membrane behaves as a pH electrode.

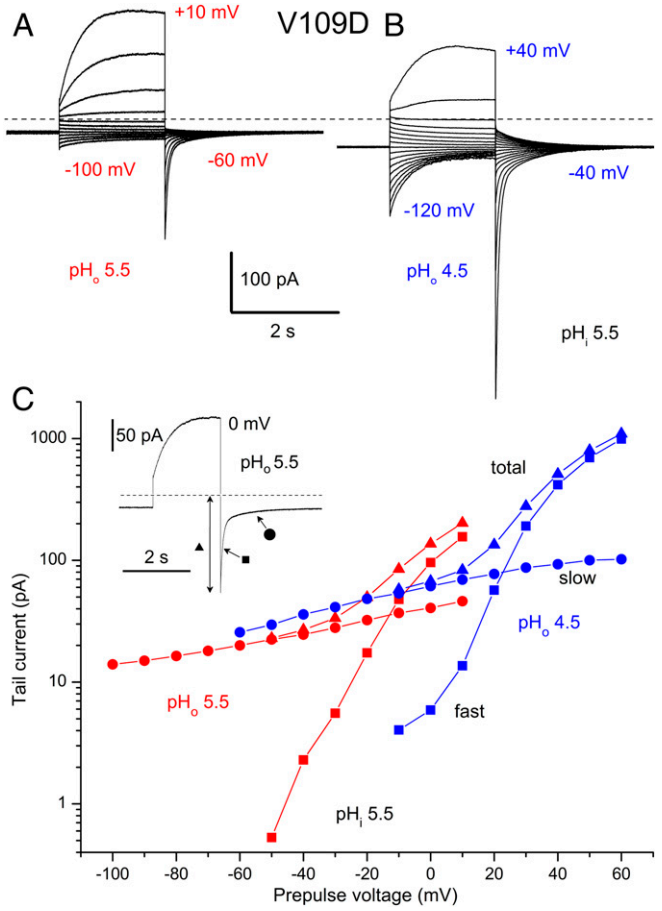

Fig. 5. Tail current kinetics in a cell with the V109D mutant reveals 2 steps in gating. (*A*) A family of currents elicited by pulses applied from V_{hold} = −60 mV to −100 through 10 mV in increments of 10 mV. The dashed line indicates zero current. Nominal pH was 5.5//5.5, but V_{rev} was −28 mV, indicating pH_i was 5.0. (*B*) A family of currents in the same cell at pH_o 4.5 during pulses from V_{hold} = −40 mV to −120 through 40 mV in 10-mV increments. Because V_{rev} was +21 mV, pH_i was 4.86. Note slow tail currents after pulses negative to V_{hold} (τ_{slow} ~ 700 ms) and that a fast tail current component appears after repolarization from voltages that activate the normal time-dependent g_H (τ_{fast} ~ 20 ms at pH_o 5.5 and 70 ms at pH_o 4.5). (*C*) Tail current amplitudes from these measurements. *Inset* identifies fast (■), slow (●), and total (▲) tail amplitudes. Slow and total are absolute "instantaneous" currents, and fast component is relative. Tails were monoexponential for negative prepulse voltages but required a double exponential for more positive prepulses.

but more positive prepulses result in mostly $C_1 \rightarrow O$ transitions. *SI Appendix*, Fig. S2 confirms that the slow decay of current at large negative voltages reflects transitions unrelated to the $C_1 \leftrightarrow O$ transition, presumably $C_1 \rightarrow C_2$.

Decreasing Hydrophobicity Outside the HG Does Not Impair Selectivity or Induce $g_{H,closed}$. Table 1 indicates whether each mutant exhibited closed-channel g_H, and its magnitude relative to the open-channel g_H, g_H(C/O). Mutations expected to decrease the hydrophobicity at positions I105, L108, L147, F150, V177, V178, or F182 did not detectably impair H^+ selectivity. Of the positions tested, the only mutations that exhibited closed-state conductance were of the 3 predicted HG residues, V109, F150, and V178, as well as V177. Because Val^{178} is the central of 5 consecutive valines, and Val^{177} obliquely faces the pore, we suspect that V177 and V178 act interchangeably. Convincing $g_{H,closed}$ was not observed for another HG neighbor (L108T) or for positions 1 helical turn above (F182A) or below the HG (I105G, I105D, L147D).

Is Phe^{182} Rather than Val^{178} Part of the HG? Homology models identify Val^{178} as part of the HG (Fig. 1), but in the crystal structure of mH_V1, this position appears to be occupied by Phe^{178} (Phe^{182} in hH_V1) (29). If the crystal structure is closer to reality than the homology models, Phe^{182} mutants might be expected to share the properties of mutations at the other 2 elements of the HG. Unfortunately, F182D mutants did not produce detectable currents, despite the transfected cells being green, indicating likely membrane expression. The lack of current in F182D may indicate that it does not face the pore in hH_V1, consistent with the homology model but not the crystal structure (Fig. 1). We then tried F182A, because a neutral substituent might be less disruptive than introducing a charge. Currents were detected and were proton selective, but convincing $g_{H,closed}$ was not detected (Table 1). In contrast, V178A, V178D, and all double or triple Ala mutants that included Val^{178} exhibited $g_{H,closed}$. That V177D also exhibits $g_{H,closed}$ further supports the role of its neighbor Val^{178} in the HG, because both are at a similar "height" in the membrane. Combined, these results strongly support the idea that Val^{178} (in concert with Val^{177}) and not Phe^{182} completes the HG in hH_V1.

The Double Mutant F150D/R211G. Our open-channel model of hH_V1 exhibited frequent interaction between F150 and R211 in the HG region, at the peak energy barrier for cation permeation (33). We therefore tested a double mutant, F150D/R211G, but it retained high proton selectivity (Table 1). Like F150D alone, this double mutant exhibited $g_{H,closed}$.

Increasing the Hydrophilicity of the HG Region Facilitates Channel Opening. Fig. 6 illustrates that most of the mutations intended to make the HG less hydrophobic accelerated channel opening. Mutation to Ala significantly accelerated activation in F150A, but mutations to Asp had greater impact. Each single Asp (V109D, F150D, V178D) mutant opened substantially faster than WT. The ubiquity of faster activation suggests that, in WT channels, the HG acts to retard channel opening. The speeding of activation and induction of $g_{H,closed}$ appear to be independent and mechanistically unrelated consequences of HG mutation. There was no correlation between the magnitude of $g_{H,closed}$ in each mutant and the speeding of τ_{act} (R^2 is 0.19 and 0.17 for linear regression on +40- or +60-mV data, respectively). Notably, some mutations (e.g., I105G, I105D, and F150A) profoundly accelerated activation, but did not produce $g_{H,closed}$. Conversely, V178A, V109A/F150A, and V109A/V178A exhibited $g_{H,closed}$ without a significant decrease in τ_{act}.

Further evidence that reducing hydrophobicity of the HG region promotes channel opening is a substantial negative shift of the g_H–V relationship in I105A and I105D (*SI Appendix*, Fig. S3). On average, the voltage at which the g_H was 10% maximal (39) shifted from 14.1 ± 3.4 mV (mean ± SEM) in 7 cells transfected with WT hH_V1 to −13.3 ± 3.6 mV (n = 7) in I105G mutants and −39.0 ± 8.3 mV (n = 5) in I105D ($P < 0.0001$ for both). We did not attempt to quantify g_H–V data for other mutants, because the additional time- and voltage-dependent $g_{H,closed}$ process **[1]** made unambiguous interpretation difficult. Other constructs did not appear as obviously shifted as Ile^{105} mutants, however. That Ile^{105} mutation produced a large negative shift without producing $g_{H,closed}$ further indicates that the 2 key functions of the HG, namely preventing proton influx through closed channels and retarding channel opening, are mechanistically independent.

The HG Prevents the Guanidinium of Arg^{208} from Moving Above Residue 150 in the Closed State. To investigate the molecular basis for closed-state proton leakiness in these HG mutants, extensive

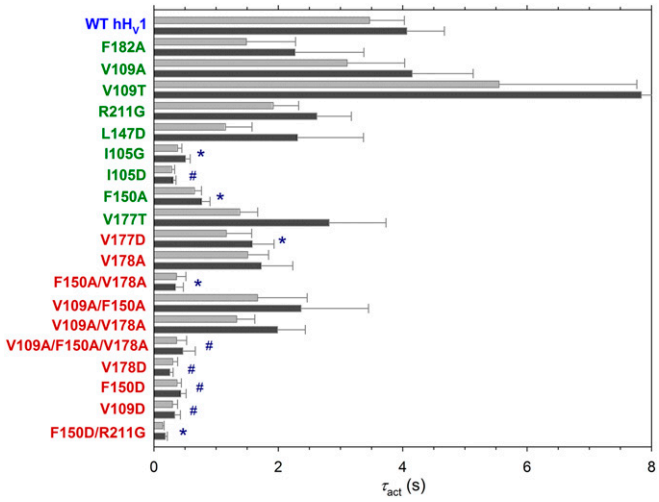

Fig. 6. Many HG mutants have faster activation kinetics. Mutants without detectable $g_{H,closed}$ are labeled in green, and those with $g_{H,closed}$ are red. Time constants of activation (τ_{act}) were determined by single- or occasionally by double-exponential fits to increasing currents. Plotted are mean ± SEM τ_{act} at 60 mV (light gray) and 40 mV (dark gray) in each mutant. When 2 exponentials were required to fit the currents reasonably, the slower one is plotted here. Significant differences from τ_{act} in WT hH_V1 indicated by $^*P < 0.05$, $^\#P < 0.01$ by Student's *t* test. *SI Appendix*, Table S2 gives statistical details of these studies. An error bar for V109T is truncated.

simulations totaling 6.5 μs were performed using the spectroscopically and biochemically constructed model of the resting state of hH_V1 by Li et al. (27). The effect of these mutations on the size and nature of the HG was analyzed by computing the average hydration along the channel (*SI Appendix*, Fig. S4). Increased pore hydration relative to WT was observed in the intracellular vestibule ($-0.9 < z < -0.5$ nm) in single aspartate mutants; however, little to no change was seen in leaky alanine mutants. Therefore, we conclude that H^+ leakiness in the closed state is not due to increased hydration of the HG.

We then monitored the position of the guanidinium group of Arg^{208} relative to the side chain of residue 150 versus the position of the S4 helix center of mass relative to the rest of the channel (S1 to S3; Fig. 7 and *SI Appendix*, Fig. S5). Consistent with the gating charge distribution of the closed state, the guanidinium group remained below Phe^{150} most of the time in the systems considered. However, transient excursions (~2 to 3 Å) of the guanidinium group of Arg^{208} above residue 150 were observed in single threonine mutants (Fig. 7*B*). These excursions became more likely in single alanine mutants (Fig. 7*C*). In double- and triple-alanine HG mutants, 2 distinct metastable conformational states were sampled in which the guanidinium group of Arg^{208} is positioned either ~1 Å above or ~1 to 2 Å below residue 150 (Fig. 7*D*). Finally, a third conformation was populated in single aspartate mutants with the side chain of Arg^{208} positioned 2 Å above Phe^{150} (Fig. 7*E*). At most, the upward shift of the Arg^{208} side chain is correlated to an 0.5- to 1-Å upward shift of the S4 helix, falling well short of the >4-Å S4 translation to the activated state in other homologous voltage sensing domains (26, 40). In our open-state model, Arg^{208} faces Asp^{112} (33). Importantly, dynamic fluctuations of the guanidinium group of Arg^{208} past residue 150 were significant and metastable in all leaky mutants but were transient and occurred very rarely in the WT channel (Fig. 7*A*) or in nonleaky mutants (Fig. 7 *B* and *C*).

Taken together, our simulation results suggest that the HG acts as a hydrophobic and steric barrier that prevents the Arg^{208} guanidinium from slipping above the gating charge transfer center in the resting state.

Discussion

The HG Retards Channel Opening in WT hH_V1. Many of the HG mutants studied activated about an order of magnitude faster

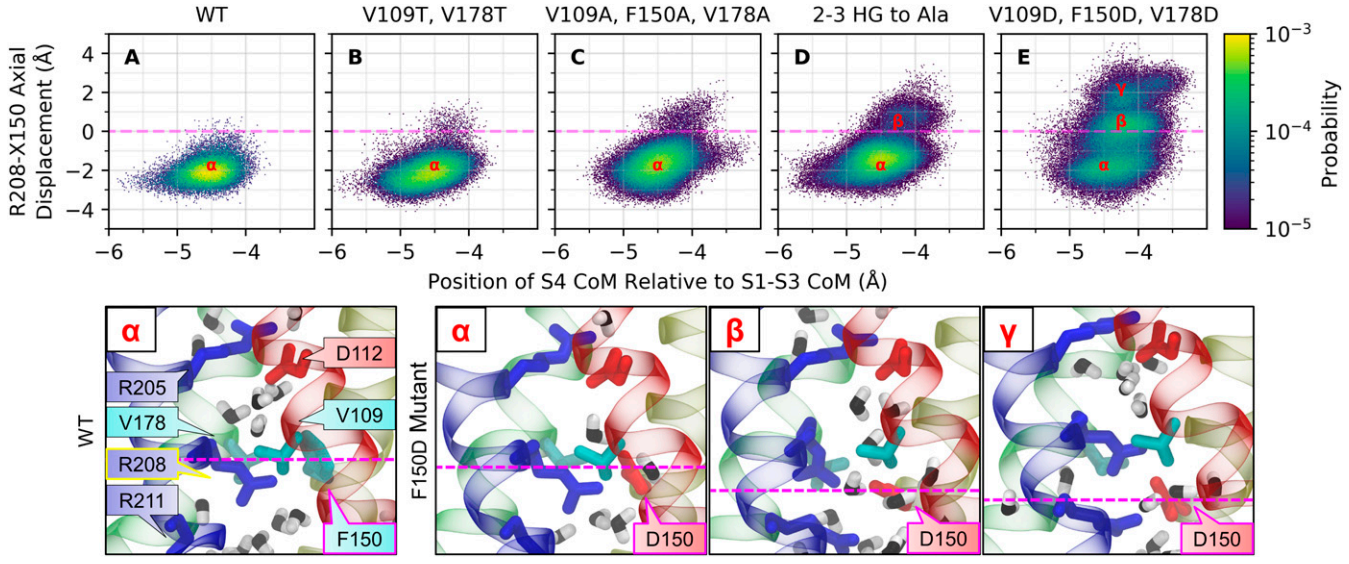

Fig. 7. Conformational fluctuations of WT and HG mutants of the resting state of hH_V1 from MD simulations. The axial position of the guanidinium group of Arg^{208} relative to the side chain of residue 150 is shown versus the axial position of the center of mass of the S4 helix relative to the center of mass (CoM) of the rest of the channel (helices S1 to S3). (*A*) WT hH_V1 samples a single basin (α), with the position of the guanidinium group remaining below residue 150 (dashed line). (*B*) Rare and transient excursions of the guanidinium group above residue 150 are observed in the (nonleaky) threonine HG mutants. (*C*) These excursions become more likely in single alanine mutants, including leaky V178A, and (*D*) populate a distinct conformational state (β) in double- and triple-alanine mutants. (*E*) Finally, aspartate mutants sample 3 distinct basins, 2 of which are located at or above residue 150 (β and γ). Representative snapshots of the single basin in WT (α) and the 3 basins (α, β, γ) in F150D are shown below the distributions. S1 (red), S2 (yellow), S3 (green), and S4 (blue) helices are shown as ribbons with side chains labeled and colored based on their residue type: hydrophobic (cyan), acidic (red), and basic (blue), with pore-associated water molecules (black). Individual distributions are included in *SI Appendix*, Fig. S5.

than WT hH_V1 (Fig. 6). This result is consistent with the report that, in V109A, F150A, and V178A, the g_H–V relationship is shifted negatively by 10 to 27 mV (41); and the present observation that activation of I105A and especially I105D are shifted dramatically toward negative values. Together, these findings indicate that the HG in WT channels impedes channel opening. Mutations in the HG region did not affect activation kinetics equally. Although most Asp mutations (I105D, V109D, F150D, V177D, and V178D) strongly accelerated opening, among the single neutral mutants only F150A (42) and I105G did. There was no correlation between the speeding of activation and the magnitude of $g_{H,closed}$, which shows that these consequences have different mechanisms. The proximity of Ile^{105} to the HG is evidently sufficient that its mutation speeds activation, but without producing $g_{H,closed}$. We conclude that activation kinetics is influenced by the overall hydrophobicity of the region, whereas inducing $g_{H,closed}$ requires decreased hydrophobicity specifically in the locations occupied by Val^{109}, Phe^{150}, Val^{177}, and Val^{178}. Surprisingly, the HG in the *Shaker* K^+ channel VSD appears to have the opposite effect on gating. Replacing Ile^{237} (which corresponds with Val^{109} in hH_V1) with less hydrophobic amino acids promoted the closed state, shifting g–V relationships positively (23).

Teleologically, that the HG resists channel opening may serve to ensure that hH_V1 opens at appropriate voltages. The ΔpH dependence of its gating means that, under all conditions, hH_V1 is poised to open just above E_H, when there is an outward electrochemical gradient for protons. Opening at more negative voltages would allow proton influx, which in most situations in most cells is deleterious.

Reducing the Hydrophobicity of the HG Produces Closed-State Proton Conduction. The most dramatic and consistent effect of reducing the hydrophobicity of HG residues was to produce a closed-channel proton-selective leak conductance. The conductance of closed channels, $g_{H,closed}$, was smaller than that of the open channel, g_H, but substantial, and dependent on many factors, especially pH_o. The magnitude of $g_{H,closed}$ increased with the number of substitutions to the HG. The single-mutant V178A had distinct but tiny $g_{H,closed}$ averaging only 1.7% of the open g_H. All 3 double Ala mutants produced moderate $g_{H,closed}$ 3 to 16% of g_H (Table 1). The triple-mutant V109A/F150A/V178A produced robust $g_{H,closed}$ (35% of g_H) comparable to that seen in V109D or F150D. We conclude that the HG in H_V1 ensures that the closed channel is fully occluded—that no ions, not even protons, are allowed into the cell.

The HG mutants still opened and closed in a voltage- and time-dependent manner, but in a voltage range negative to that producing normal time-dependent gating, closed channels allowed continuous proton influx. It might be argued that these mutations disrupt the integrity of the protein or disturb gating, and that consequently the proton leak is not very meaningful, simply indicating a broken channel. Three observations argue against this interpretation. First, these mutants still exhibited voltage- and time-dependent gating, suggesting that the gating mechanism was not grossly altered. Second, the strong proton selectivity of the closed-channel leak conductance suggests that the selectivity filter remained intact. Proton-selective conduction occurs only under the specific conditions of an appropriately juxtaposed Asp in S1 and Arg in S4 (43–45), and thus requires integrity of the selectivity filter of mutant proteins. Finally, potent Zn^{2+} inhibition of depolarization-activated H^+ current suggests that the Zn^{2+} binding site remained largely intact. In WT hH_V1 Zn^{2+} is coordinated tetrahedrally by His^{140}, His^{193}, Asp^{123}, and Glu^{119} (residues residing on S1, S2, and the S3–S4 linker) based on mutation studies (12, 36), IR spectroscopy (46), and on the X-ray structure of the mH_V1 crystal, which included a Zn^{2+} atom at its external binding site (29). That Zn^{2+} still potently inhibits both closed- and open-channel currents supports the idea that the HG mutants were globally functionally intact.

Which Amino Acids Comprise the HG? Homology models identify Val^{178} as part of the HG (Fig. 1), analogous to Ile^{190} in CiVSP or Ile^{320} in *Shaker* (28, 47). However, in the crystal structure of mH_V1, this position appears to be occupied by Phe^{178} (Phe^{182} in hH_V1), in a region called the inner hydrophobic layer (29). A subsequent EPR study of hH_V1 concluded that in the crystal structure of mH_V1, replacing a 25-amino acid region of S2 through S3 with amino acids spliced from CiVSP resulted in a register shift of 1 turn of the helix up for S2 helix and down for S3 (27). When the crystal structure is "corrected" for these shifts, Val^{178} aligns with Phe^{150} and Val^{109} to complete the HG (27), as shown in Fig. 1*B*. Given this ambiguity, we mutated Phe^{182} in hH_V1. If the crystal structure is closer to reality than the homology models, Phe^{182} mutants might be expected to share the manifestations of mutations to the other 2 HG elements. The F182D mutant did not produce detectable currents, despite the transfected cells being green, indicating likely membrane expression. In a previous study, we introduced Asp at each of 11 contiguous locations along the S1 transmembrane helix and observed current only with Asp at the 3 positions judged to face the pore in our homology model (43). Although other explanations are possible, the lack of current in F182D may indicate that it does not face the pore in hH_V1, consistent with homology model predictions (27). The less obtrusive F182A mutant generated proton-selective currents but exhibited no $g_{H,closed}$. We conclude that Val^{178} and not Phe^{182} is part of the HG.

To further define the location of the HG, we mutated hydrophobic residues that face the pore in the model and reside 1 helical turn above (Leu^{147}, Phe^{182}) or below (Ile^{105}) the putative HG. All remained proton selective and none exhibited detectable $g_{H,closed}$. It is surprising that L147T or L147D did not, because at the corresponding *Shaker* position, I287H does leak protons (22), but position 147 in S2 of hH_V1 is at the level of Asp^{112}, the selectivity filter (30), which has no parallel in the *Shaker* VSD. We mutated Val^{177}, which neighbors Val^{178}, the central member of a string of 5 valines. In a closed hH_V1 model (27), Val^{178} faces the pore directly, but with a small rotation Val^{177} would face the pore. V177D produced a distinct $g_{H,closed}$ with faster activation. Evidently decreasing the hydrophobicity of either Val^{178} or Val^{177} compromises the closed channel. Taken together, these results support the identification of the HG in hH_V1 as Val^{109}, Phe^{150}, Val^{177}, and Val^{178}.

What Is the Proton-Selective Pathway through Closed HG Mutant Channels? One might imagine that decreased hydrophobicity in the HG region allows a more continuous water wire or, in the case of Asp mutants (V109D, F150D, V177D, and V178D), may directly create a proton transfer site. MD simulations in the closed-channel model show little change in hydration (*SI Appendix*, Fig. S4) and also indicate that the most hydrophobic region of the pore and the peak of the energetic barrier to cation permeation in the open state are at the level of the HG (33, 43, 45) (*SI Appendix*, Fig. S1). This led to the hypothesis that the HG might contribute to the exquisite proton selectivity of H_V1, but this prediction was not borne out, as the HG mutants retained H^+ selectivity.

Proton translocation in protein interiors is thought to occur by means of a Grotthuss relay mechanism along hydrogen-bonded chains of water molecules and titratable groups (35, 38, 48, 49). The involvement of water in H_V1 permeation is ambiguous (50–52). The closed mH_V1 crystal structure (29) and a closed CiH_V1 channel model (53) contain 2 hydrophobic regions. However, open-channel models also exhibit hydrophobic regions (33, 45) that do not obviously differ in presumed closed states (50) or in Asp^{112} mutants that conduct protons, anions, or nothing (43). The present results demonstrate that the HG region alone is sufficient

to preclude H^+ conduction in closed hH_V1 channels, and furthermore, that other bottlenecks are not.

The fact that closed hH_V1 channels conduct protons if the HG is made less hydrophobic, even by single point mutations, is consistent with the view that the physical barrier separating protons from one side of the closed channel to the other is relatively thin. Also consistent with this view is the observation that the R205H mutant of hH_V1 can conduct protons at negative voltages where the channel is presumably closed (25). A crucial property of the HG in other channels is that most of the membrane potential drops across this relatively short distance (~4 to 10 Å) (17–21, 54–56). Consequently, charged groups that move through the HG essentially transfer their charge from intracellular to extracellular while moving across only a fraction of the membrane thickness. Steep voltage dependence can thus be achieved with limited physical movement, illustrating the parsimony of natural selection. Like other VSDs, H_V1 has a focused electric field that enables gating with minimal motion of the protein.

It is clear that a conserved Asp in the middle of the S1 transmembrane helix is crucial for the H^+ selectivity of H_V1, because mutations that neutralize Asp result in anion permeability in 3 species (3, 30, 57). In most open-state homology models, Asp interacts almost continuously with one or more Arg in S4 (33, 43, 45, 53, 58), while quantum mechanical calculations on a reduced model of the H_V1 selectivity filter showed that Asp–Arg interaction can explain both proton permeation and proton selectivity (44). That $g_{H,closed}$ is proton selective supports the idea that the sole selectivity filter, comprising Asp^{112} in S1 interacting with one or more Arg from S4, remains intact in the (C_1) closed state of hH_V1.

H^+ Leakiness in HG Mutants Is Due to a More Open-Like Conformation in the Resting State. Consistent with the above considerations on the nature and the thickness of the barrier opposing proton permeation in the resting state of the channel, the HG mutants in which the guanidinium group of Arg^{208} was most likely to slip past residue 150 correspond to the experimentally determined H^+ leaky mutants (Fig. 7 and *SI Appendix*, Fig. S5). In this compromised conformational state, the channel topologically resembles the activated state in that Arg^{208} faces the extracellular vestibule of the pore, with a gating charge distribution intermediate between that of the closed state, in which Arg^{208} sits below Phe^{150} in the intracellular vestibule, and that of the open state, in which Arg^{208} is near Asp^{112} in the extracellular vestibule. These results suggest that H^+ leakiness in HG mutants is a result of the inability of the gasket to prevent the guanidinium group of Arg^{208} from crossing the charge transfer center in a process where reduced steric interactions and new charge–charge interactions compromise the integrity of the HG.

Why Does Zn^{2+} Inhibit Closed-Channel H^+ Current? The bulk of evidence supports the idea that Zn^{2+} inhibits WT hH_V1 currents by binding to the closed WT hH_V1 channel and preventing opening (59–61). In a recent proposal, protons permeate hH_V1 by binding consecutively to 3 sites, each with 2 acidic groups; the internal site includes E153 and D174, the central site D112 and D185, and the outer site E119 and D123 (62). Although the amino acids most critical for Zn^{2+} binding to mammalian H_V1 are His^{140} and His^{193} (12, 29, 36), the crystal structure of the closed mH_V1 also implicates E119 and D123 in Zn^{2+} coordination (29). Thus, both acids comprising the external proton binding site (62) would be busy binding Zn^{2+}, and unavailable to shuttle protons out of the pore. Because E119 and D123 are both on S1, their relative positions would likely be uninfluenced by opening or closing of the channel. Although decreased hydrophobicity of HG mutants allows proton permeation through the HG constriction in closed (C_1) channels, the proton might still need the outer pair of acids to complete its journey. Despite the attractiveness of this mechanism, we cannot rule out an alternative possibility that Zn^{2+} inhibits closed-channel H^+ current by the simple fact of binding in the outer vestibule and occluding the proton pathway by electrostatic repulsion and steric obstruction.

Implications for Gating Mechanisms. We present strong evidence for at least 2 distinct closed states, consistent with many previous studies proposing multiple gating states (31, 37, 42, 63–67). That the shallow C_1 closed state conducts protons in HG mutants uniquely enables distinguishing this state electrophysiologically. Because a variety of mutations produced similar phenomenology, it appears that the gating mechanism itself was not grossly altered; hence, the C_1 state likely exists in WT channels. At voltages negative to the normal gating process, larger hyperpolarization produced a slow tail current indicating a second closing step (Fig. 5). The voltage dependence of this ($C_1 \leftrightarrow C_2$) gating process is extremely weak. Similarly, Cherny et al. (37) observed a steeply voltage-dependent closing process in rat H_V1 near threshold voltages, with a weakly voltage-dependent component at more negative voltages. Several previous studies have concluded that most of the gating charge moves between closed states, prior to the opening transition (25, 65–67). The weak voltage dependence of $C_2 \leftrightarrow C_1$ transitions and the steep voltage dependence of the $C_1 \leftrightarrow O$ step (Fig. 5 and *SI Appendix*, Fig. S2) observed here appear to contradict this conclusion, although the $C_1 \leftrightarrow O$ step may encompass several substates of a more complete model. An intriguing possibility is that the deep closed-state C_2 occurs when extreme hyperpolarization traps Arg^{208} below the HG where it resides in WT hH_V1 (Fig. 7*A*).

Many if not most gated ion channels contain a hydrophobic gate that undergoes sharp wetting and dewetting transitions resulting from conformational changes upon opening and closing, respectively (53, 68–71). Whether or not the HG functions as a hydrophobic gate in H_V1 is unclear. First, hydrophobic gates tend to extend over distances of 1 to 1.5 nm, longer than the length of the HG. Second, we did not find systematic differences in hydration between HG mutants exhibiting proton permeation or not (*SI Appendix*, Fig. S4). Previously, we found hydration to be indistinguishable in H^+-selective, anion-selective, and nonconducting hH_V1 mutants (43). It is possible that the HG widens upon opening (53) or that open and closed states differ in side-chain orientations (27). In light of the ΔpH dependence of H_V1 activation (37), protonation of internal residues at low pH_i or deprotonation of external residues at high pH_o might alter the channel conformation in a way that permits proton permeation. Answering these questions will require detailed comparisons of open and closed states of the channel.

Implications for Genetic Disease. Intriguingly, episodic ataxia in the human $K_V1.1$ channel is associated with mutations at positions corresponding to Val^{109} (72) and Val^{178} (73) in hH_V1. We predict that an individual with mutations to HG residues in hH_V1 might exhibit closed-channel proton current. We and others (22, 25) have noticed that mutations that produce constitutive proton leak seem to decrease the vitality and longevity of cells that express these channels. Specific mutations to the VSD of other voltage-gated ion channels produce "omega currents" or "gating pore currents" in which the VSD becomes permeable to protons (74) or simply to cations in general. These gating pore currents are associated with a variety of hereditary diseases that mostly afflict excitable cells, nerve and muscle (75). The COSMIC database (76) has an entry for an F150C mutation in the HVCN1 gene from a 70-y-old male with bladder carcinoma, raising intriguing possibilities for future study.

Materials and Methods

MD Simulations. MD methods are provided in *SI Appendix*.

Gene Expression. Site-directed mutants were created using the Stratagene QuikChange (Agilent) procedure according to the manufacturer's instructions. Transfection into HEK-293 cells was done as described (33). The following mutants were produced by GenScript: L147D, F150A, F150D, R211G, F150D/R211G, V109A/F150A/V178A, and V109A/V178A. No other voltage- or time-dependent conductances were observed under the conditions of this study. Most mutations were introduced into the WT background. In a few cases, mutations were introduced into a Zn^{2+}-insensitive background (H140A/H193A), which we have used previously to distinguish the mutant channels from endogenous H_V1 (30). In most cases, the level of expression of all mutants studied here was sufficiently high that contamination by native H_V1 was negligible.

Electrophysiology. In most experiments, cells expressing GFP-tagged proton channels were identified using Nikon inverted microscopes with fluorescence capability. For constructs that lacked the GFP tag, GFP was cotransfected. Conventional patch-clamp techniques were used (33) at room temperature (20 to 26 °C). Bath and pipette solutions contained 60 to 100 mM buffer, 1 to 2 mM $CaCl_2$ or $MgCl_2$ (intracellular solutions were Ca^{2+}-free), 1 to 2 mM EGTA, and $TMAMeSO_3$ to adjust the osmolality to ~300 mOsm, titrated with TMAOH. Buffers used were Homopipes at pH 4.5 to 5.0, Mes at pH 5.5 to 6.0, BisTris at pH 6.5, Pipes at pH 7.0, Hepes at pH 7.5, and Tricine at pH 8.0. Currents are shown without leak correction. To minimize pH_i changes due to large H^+ fluxes, pulses for large depolarizations in pulse families were sometimes shortened. Reversal potentials (V_{rev}) were determined by 2 methods, as described previously (77).

Closed-Channel Conduction. Proton current amplitude (I_H) was usually determined by fitting the rising current with a single exponential and extrapolating to infinite time. Proton conductance (g_H) was calculated from I_H and V_{rev} measured in each solution, which was often well negative to the nominal E_H: $g_H = I_H/(V - V_{rev})$. The open-state g_H was calculated from the largest outward current measured. In some cases where current activation kinetics was difficult to evaluate, g_H was calculated from tail current amplitudes instead of I_H. Closed-channel g_H ($g_{H,closed}$) was calculated in 2 different ways, depending on its amplitude. In mutants in which $g_{H,closed}$ was small, it was calculated from the holding current, usually at −40 mV, and V_{rev} measured under the same conditions, ignoring any non-H^+ leak. For this purpose, V_{rev} was simply the zero current potential, which was typically similar or identical to that determined using tail currents. If both open and closed conductances are proton selective, their V_{rev} should be the same. There were no instances in which these values were convincingly different, except in leaky cells. Cells with large leak currents were excluded from analysis. Without an objective way to estimate genuine leak, it is likely that $g_{H,closed}$ is systematically overestimated. In cells with large $g_{H,closed}$, we estimated its relative amplitude ($g_{H,closed}/g_H$) from the difference between the initial and final current during a large depolarizing pulse ($I_{t\,=\,0}/I_{t=\infty}$), again ignoring leak. This value does not require knowledge of V_{rev} and also is not affected by intrinsic rectification of the $g_{H,closed}$ current–voltage relationship. Because this method does not correct for leak it will tend to overestimate the ratio. Because Zn^{2+} inhibited most of the holding current, we image the error is not inordinate. It should be emphasized that these estimates are rather arbitrary and will depend on V_{hold} and pH, as well as pipette geometry, cell volume, nonproton leak current, the completeness of equilibration, and the assumptions that all channels at V_{hold} are in $Closed_1$ (not $Closed_2$) and all proceed to *Open* during a large depolarization **[1]**.

ACKNOWLEDGMENTS. This work was supported by National Institutes of Health Grant GM102336 (to T.E.D. and S.M.E.S.), National Institutes of Health Grants GM121462 and GM126902 (to T.E.D.), National Science Foundation Grant MCB-0943362 (to T.E.D. and S.M.E.S.), Bears Care (D.M.), Deutsche Forschungsgemeinschaft Grant MU 3574/4-1 (to B.M.), and Canadian Institutes of Health Research Grant MOP-130461 (to R.P.). The content is solely the responsibility of the authors and does not necessarily represent the official views of the National Institutes of Health. The authors appreciate detailed criticism by Valerij Sokolov, and thank Qufei (Francis) Li and Eduardo Perozo for providing structural information.

1. A. R. Taylor, A. Chrachri, G. Wheeler, H. Goddard, C. Brownlee, A voltage-gated H^+ channel underlying pH homeostasis in calcifying coccolithophores. *PLoS Biol.* **9**, e1001085 (2011).
2. J. D. Rodriguez *et al*., Identification of a vacuolar proton channel that triggers the bioluminescent flash in dinoflagellates. *PLoS One* **12**, e0171594 (2017).
3. S. M. E. Smith *et al*., Voltage-gated proton channel in a dinoflagellate. *Proc. Natl. Acad. Sci. U.S.A.* **108**, 18162–18167 (2011).
4. T. E. DeCoursey, Voltage-gated proton channels: Molecular biology, physiology, and pathophysiology of the H_V family. *Physiol. Rev.* **93**, 599–652 (2013).
5. T. E. DeCoursey, Voltage-gated proton channels find their dream job managing the respiratory burst in phagocytes. *Physiology (Bethesda)* **25**, 27–40 (2010).
6. T. E. DeCoursey, D. Morgan, V. V. Cherny, The voltage dependence of NADPH oxidase reveals why phagocytes need proton channels. *Nature* **422**, 531–534 (2003).
7. L. M. Henderson, J. B. Chappell, O. T. G. Jones, The superoxide-generating NADPH oxidase of human neutrophils is electrogenic and associated with an H^+ channel. *Biochem. J.* **246**, 325–329 (1987).
8. D. Morgan *et al*., Voltage-gated proton channels maintain pH in human neutrophils during phagocytosis. *Proc. Natl. Acad. Sci. U.S.A.* **106**, 18022–18027 (2009).
9. I. S. Ramsey, E. Ruchti, J. S. Kaczmarek, D. E. Clapham, Hv1 proton channels are required for high-level NADPH oxidase-dependent superoxide production during the phagocyte respiratory burst. *Proc. Natl. Acad. Sci. U.S.A.* **106**, 7642–7647 (2009).
10. A. El Chemaly *et al*., VSOP/Hv1 proton channels sustain calcium entry, neutrophil migration, and superoxide production by limiting cell depolarization and acidification. *J. Exp. Med.* **207**, 129–139 (2010).
11. P. V. Lishko, I. L. Botchkina, A. Fedorenko, Y. Kirichok, Acid extrusion from human spermatozoa is mediated by flagellar voltage-gated proton channel. *Cell* **140**, 327–337 (2010).
12. I. S. Ramsey, M. M. Moran, J. A. Chong, D. E. Clapham, A voltage-gated proton-selective channel lacking the pore domain. *Nature* **440**, 1213–1216 (2006).
13. M. Sasaki, M. Takagi, Y. Okamura, A voltage sensor-domain protein is a voltage-gated proton channel. *Science* **312**, 589–592 (2006).
14. F. Papp *et al*., TMEM266 is a functional voltage sensor regulated by extracellular Zn^{2+}. *eLife* **8**, e42372 (2019).
15. S. Y. Lee, J. A. Letts, R. MacKinnon, Functional reconstitution of purified human Hv1 H^+ channels. *J. Mol. Biol.* **387**, 1055–1060 (2009).
16. N. Yang, R. Horn, Evidence for voltage-dependent S4 movement in sodium channels. *Neuron* **15**, 213–218 (1995).
17. N. Yang, A. L. George, Jr, R. Horn, Molecular basis of charge movement in voltage-gated sodium channels. *Neuron* **16**, 113–122 (1996).
18. H. P. Larsson, O. S. Baker, D. S. Dhillon, E. Y. Isacoff, Transmembrane movement of the *Shaker* K^+ channel S4. *Neuron* **16**, 387–397 (1996).
19. D. M. Starace, E. Stefani, F. Bezanilla, Voltage-dependent proton transport by the voltage sensor of the *Shaker* K^+ channel. *Neuron* **19**, 1319–1327 (1997).
20. D. M. Starace, F. Bezanilla, Histidine scanning mutagenesis of basic residues of the S4 segment of the *Shaker* K^+ channel. *J. Gen. Physiol.* **117**, 469–490 (2001).
21. D. M. Starace, F. Bezanilla, A proton pore in a potassium channel voltage sensor reveals a focused electric field. *Nature* **427**, 548–553 (2004).
22. F. V. Campos, B. Chanda, B. Roux, F. Bezanilla, Two atomic constraints unambiguously position the S4 segment relative to S1 and S2 segments in the closed state of Shaker K channel. *Proc. Natl. Acad. Sci. U.S.A.* **104**, 7904–7909 (2007).
23. J. J. Lacroix, H. C. Hyde, F. V. Campos, F. Bezanilla, Moving gating charges through the gating pore in a Kv channel voltage sensor. *Proc. Natl. Acad. Sci. U.S.A.* **111**, E1950–E1959 (2014).
24. X. Tao, A. Lee, W. Limapichat, D. A. Dougherty, R. MacKinnon, A gating charge transfer center in voltage sensors. *Science* **328**, 67–73 (2010).
25. A. L. Randolph, Y. Mokrab, A. L. Bennett, M. S. Sansom, I. S. Ramsey, Proton currents constrain structural models of voltage sensor activation. *eLife* **5**, e18017 (2016).
26. Q. Li *et al*., Structural mechanism of voltage-dependent gating in an isolated voltage-sensing domain. *Nat. Struct. Mol. Biol.* **21**, 244–252 (2014).
27. Q. Li *et al*., Resting state of the human proton channel dimer in a lipid bilayer. *Proc. Natl. Acad. Sci. U.S.A.* **112**, E5926–E5935 (2015).
28. T. E. DeCoursey, Structural revelations of the human proton channel. *Proc. Natl. Acad. Sci. U.S.A.* **112**, 13430–13431 (2015).
29. K. Takeshita *et al*., X-ray crystal structure of voltage-gated proton channel. *Nat. Struct. Mol. Biol.* **21**, 352–357 (2014).
30. B. Musset *et al*., Aspartate 112 is the selectivity filter of the human voltage-gated proton channel. *Nature* **480**, 273–277 (2011).
31. C. Gonzalez, S. Rebolledo, M. E. Perez, H. P. Larsson, Molecular mechanism of voltage sensing in voltage-gated proton channels. *J. Gen. Physiol.* **141**, 275–285 (2013).
32. E. F. Pettersen *et al*., UCSF Chimera—a visualization system for exploratory research and analysis. *J. Comput. Chem.* **25**, 1605–1612 (2004).
33. K. Kulleperuma *et al*., Construction and validation of a homology model of the human voltage-gated proton channel hH_V1. *J. Gen. Physiol.* **141**, 445–465 (2013).
34. T. E. DeCoursey, Hydrogen ion currents in rat alveolar epithelial cells. *Biophys. J.* **60**, 1243–1253 (1991).
35. T. E. DeCoursey, J. Hosler, Philosophy of voltage-gated proton channels. *J. R. Soc. Interface* **11**, 20130799 (2013).
36. B. Musset *et al*., Zinc inhibition of monomeric and dimeric proton channels suggests cooperative gating. *J. Physiol.* **588**, 1435–1449 (2010).
37. V. V. Cherny, V. S. Markin, T. E. DeCoursey, The voltage-activated hydrogen ion conductance in rat alveolar epithelial cells is determined by the pH gradient. *J. Gen. Physiol.* **105**, 861–896 (1995).
38. T. E. DeCoursey, Voltage-gated proton channels and other proton transfer pathways. *Physiol. Rev.* **83**, 475–579 (2003).
39. V. V. Cherny *et al*., Tryptophan 207 is crucial to the unique properties of the human voltage-gated proton channel, hH_V1. *J. Gen. Physiol.* **146**, 343–356 (2015).

40. A. Nekouzadeh, Y. Rudy, Conformational changes of an ion-channel during gating and emerging electrophysiologic properties: Application of a computational approach to cardiac Kv7.1. *Prog. Biophys. Mol. Biol.* **120**, 18–27 (2016).
41. L. Hong, I. H. Kim, F. Tombola, Molecular determinants of Hv1 proton channel inhibition by guanidine derivatives. *Proc. Natl. Acad. Sci. U.S.A.* **111**, 9971–9976 (2014).
42. L. Hong, M. M. Pathak, I. H. Kim, D. Ta, F. Tombola, Voltage-sensing domain of voltage-gated proton channel Hv1 shares mechanism of block with pore domains. *Neuron* **77**, 274–287 (2013).
43. D. Morgan *et al*., Peregrination of the selectivity filter delineates the pore of the human voltage-gated proton channel hH_V1. *J. Gen. Physiol.* **142**, 625–640 (2013).
44. T. Dudev *et al*., Selectivity mechanism of the voltage-gated proton channel, H_V1. *Sci. Rep.* **5**, 10320 (2015).
45. A. Chamberlin, F. Qiu, Y. Wang, S. Y. Noskov, H. P. Larsson, Mapping the gating and permeation pathways in the voltage-gated proton channel Hv1. *J. Mol. Biol.* **427**, 131–145 (2015).
46. M. Iwaki *et al*., Zn^{2+}-binding to the voltage-gated proton channel Hv1/VSOP. *J. Phys. Chem. B* **122**, 9076–9080 (2018).
47. T. E. DeCoursey, D. Morgan, B. Musset, V. V. Cherny, Insights into the structure and function of H_V1 from a meta-analysis of mutation studies. *J. Gen. Physiol.* **148**, 97–118 (2016).
48. J. F. Nagle, H. J. Morowitz, Molecular mechanisms for proton transport in membranes. *Proc. Natl. Acad. Sci. U.S.A.* **75**, 298–302 (1978).
49. R. Pomès, B. Roux, Structure and dynamics of a proton wire: A theoretical study of H^+ translocation along the single-file water chain in the gramicidin A channel. *Biophys. J.* **71**, 19–39 (1996).
50. E. Gianti, L. Delemotte, M. L. Klein, V. Carnevale, On the role of water density fluctuations in the inhibition of a proton channel. *Proc. Natl. Acad. Sci. U.S.A.* **113**, E8359–E8368 (2016).
51. A. L. Bennett, I. S. Ramsey, CrossTalk opposing view: Proton transfer in Hv1 utilizes a water wire, and does not require transient protonation of a conserved aspartate in the S1 transmembrane helix. *J. Physiol.* **595**, 6797–6799 (2017).
52. T. E. DeCoursey, CrossTalk proposal: Proton permeation through H_V 1 requires transient protonation of a conserved aspartate in the S1 transmembrane helix. *J. Physiol.* **595**, 6793–6795 (2017).
53. A. Chamberlin *et al*., Hydrophobic plug functions as a gate in voltage-gated proton channels. *Proc. Natl. Acad. Sci. U.S.A.* **111**, E273–E282 (2014).
54. L. D. Islas, F. J. Sigworth, Electrostatics and the gating pore of Shaker potassium channels. *J. Gen. Physiol.* **117**, 69–89 (2001).
55. F. Tombola, M. M. Pathak, E. Y. Isacoff, Voltage-sensing arginines in a potassium channel permeate and occlude cation-selective pores. *Neuron* **45**, 379–388 (2005).
56. C. A. Ahern, R. Horn, Focused electric field across the voltage sensor of potassium channels. *Neuron* **48**, 25–29 (2005).
57. G. Chaves *et al*., Identification of an H_V1 voltage-gated proton channel in insects. *FEBS J.* **283**, 1453–1464 (2016).
58. M. L. Wood *et al*., Water wires in atomistic models of the Hv1 proton channel. *Biochim. Biophys. Acta* **1818**, 286–293 (2012).
59. V. V. Cherny, T. E. DeCoursey, pH-dependent inhibition of voltage-gated H^+ currents in rat alveolar epithelial cells by Zn^{2+} and other divalent cations. *J. Gen. Physiol.* **114**, 819–838 (1999).
60. F. Qiu *et al*., Molecular mechanism of Zn^{2+} inhibition of a voltage-gated proton channel. *Proc. Natl. Acad. Sci. U.S.A.* **113**, E5962–E5971 (2016).
61. V. De La Rosa, A. L. Bennett, I. S. Ramsey, Coupling between an electrostatic network and the Zn^{2+} binding site modulates Hv1 activation. *J. Gen. Physiol.* **150**, 863–881 (2018).
62. S. C. van Keulen *et al*., Does proton conduction in the voltage-gated H^+ channel hHv1 involve Grotthuss-like hopping via acidic residues? *J. Phys. Chem. B* **121**, 3340–3351 (2017).
63. T. E. DeCoursey, V. V. Cherny, Voltage-activated hydrogen ion currents. *J. Membr. Biol.* **141**, 203–223 (1994).
64. F. Tombola, M. H. Ulbrich, S. C. Kohout, E. Y. Isacoff, The opening of the two pores of the Hv1 voltage-gated proton channel is tuned by cooperativity. *Nat. Struct. Mol. Biol.* **17**, 44–50 (2010).
65. F. Qiu, S. Rebolledo, C. Gonzalez, H. P. Larsson, Subunit interactions during cooperative opening of voltage-gated proton channels. *Neuron* **77**, 288–298 (2013).
66. C. A. Villalba-Galea, Hv1 proton channel opening is preceded by a voltage-independent transition. *Biophys. J.* **107**, 1564–1572 (2014).
67. E. M. Carmona *et al*., Gating charge displacement in a monomeric voltage-gated proton (H_V1) channel. *Proc. Natl. Acad. Sci. U.S.A.* **115**, 9240–9245 (2018).
68. J. Zimmerberg, F. Bezanilla, V. A. Parsegian, Solute inaccessible aqueous volume changes during opening of the potassium channel of the squid giant axon. *Biophys. J.* **57**, 1049–1064 (1990).
69. N. Unwin; The Croonian Lecture, The Croonian Lecture 2000. Nicotinic acetylcholine receptor and the structural basis of fast synaptic transmission. *Philos. Trans. R. Soc. Lond. B Biol. Sci.* **355**, 1813–1829 (2000).
70. M. Yamashita *et al*., STIM1 activates CRAC channels through rotation of the pore helix to open a hydrophobic gate. *Nat. Commun.* **8**, 14512 (2017).
71. S. Rao *et al*., Water and hydrophobic gates in ion channels and nanopores. *Faraday Discuss.* **209**, 231–247 (2018).
72. P. Imbrici, M. C. D'Adamo, D. M. Kullmann, M. Pessia, Episodic ataxia type 1 mutations in the KCNA1 gene impair the fast inactivation properties of the human potassium channels Kv1.4-1.1/Kvβ1.1 and Kv1.4-1.1/Kvβ1.2. *Eur. J. Neurosci.* **24**, 3073–3083 (2006).
73. J. Zhu, R. Alsaber, J. Zhao, E. Ribeiro-Hurley, W. B. Thornhill, Characterization of the Kv1.1 I262T and S342I mutations associated with episodic ataxia 1 with distinct phenotypes. *Arch. Biochem. Biophys.* **524**, 99–105 (2012).
74. A. F. Struyk, S. C. Cannon, A Na^+ channel mutation linked to hypokalemic periodic paralysis exposes a proton-selective gating pore. *J. Gen. Physiol.* **130**, 11–20 (2007).
75. A. Moreau, P. Gosselin-Badaroudine, M. Chahine, Biophysics, pathophysiology, and pharmacology of ion channel gating pores. *Front. Pharmacol.* **5**, 53 (2014).
76. S. A. Forbes *et al*., COSMIC: Somatic cancer genetics at high-resolution. *Nucleic Acids Res.* **45**, D777–D783 (2017).
77. D. Morgan, T. E. DeCoursey, Analysis of electrophysiological properties and responses of neutrophils. *Methods Mol. Biol.* **1124**, 121–158 (2014).